Rock Mechanics and Rock Engineering (2023) 56:3843–3855
https://doi.org/10.1007/s00603-023-03252-z

TECHNICAL NOTE

Insights From a Combined Analysis of Acoustic Emission Signals for Water-Bearing Rocks in Four-Point Bending Tests: Failure Mode Classification and Strength Degradation

Jun Zhu[1,2] · **Jianhui Deng**[2]

Received: 4 October 2022 / Accepted: 24 January 2023 / Published online: 7 February 2023

Highlights

- Water-bearing causes substantial reductions in the tensile strength of rocks under four-point bending.
- There is an obvious correlation between dominant frequency bands of acoustic emission waveform and failure modes.
- The water-bearing effect on rock tensile strength can be characterized by the failure components associated with it.
- Tensile strength degradation of rocks under four-point bending can be attributed to friction weakening and fracture energy reduction.

Keywords Acoustic emission · Combined analysis · Water bearing · Failure mode classification · Strength degradation · Four-point bending tests

1 Introduction

The acoustic emission (AE) technique is characterized by non-destructive and passive monitoring and is widely used to evaluate the physical conditions and intrinsic progressive failure of rock materials (Manthei and Eisenblätter 2008; Rodríguez and Celestino 2019). AE signals, defined as transient elastic waves, are produced during the microcracking propagation when rock is subjected to a sufficiently large stress. Among the early studies on AE signals, the largest published sets of experimental results are related to parameter analysis, such as evaluations of the magnitude of in situ stress (the application of the Kaiser effect) and the safety of engineering structures by AE counts and energy (Li and Nordlund 1993; Wang et al. 2000). This approach, parameter-based namely, consumes less time and storage space to process AE signal data and thus has played a vital role in evaluating the damage severity and fracture of rocks for a long time.

Thanks to the overwhelming improvement of sensors and processors, spectrum analysis of enormous AE waveform signals emitted from rock fracturing has been gradually popularized and some important features, e.g., double dominant frequency bands, have been found. Chugh et al. (1968) analyzed the AE spectrum of Crab-Orchard sandstone, Indiana limestone, and Barre granite under direct tension, and found that the dominant frequencies of AE signals are mainly distributed in the ranges of 0 ~ 6 and 10 ~ 15 kHz. Jia (2013) comprehensively studied the AE spectrum characteristics of five rocks in the rock burst tests using AE sensors with narrowband and wideband. Two dominant frequency bands (i.e., 30 ~ 90 and 170 ~ 190 kHz) were observed in tests with narrowband sensors, and low frequency or middle-low frequency of AE signals was shown in tests with wideband sensors. According to Zhang et al. (2014), the dominant frequency of AE waveforms shifted from low-frequency bands to high-frequency bands with the increase of applied load, and the amplitude of the dominant frequency generally showed a decreasing trend. In a similar manner, He et al. (2015) and Zhang et al. (2016) reported the two dominant

✉ Jun Zhu
zhujun@imde.ac.cn

[1] Key Laboratory of Mountain Hazards and Earth Surface Process, Institute of Mountain Hazards and Environment, Chinese Academy of Sciences (CAS), Chengdu 610299, China

[2] State Key Laboratory of Hydraulics and Mountain River Engineering, College of Water Resources and Hydropower, Sichuan University, Chengdu 610065, China

frequency bands of AE waveforms of limestone under triaxial compression and granite under splitting load, respectively. It should be noted that the limitations of the above studies are: (1) insufficient statistical analysis because of limited AE signals recorded, and (2) simple loading regime for a certain rock type. To circumvent these limitations, Deng et al. (2018) and Li (2017) studied the AE waveform signals generated by various hard rocks, including marble, limestone, basalt, diorite, and granite, under a wide range of test conditions (i.e., direct tension, splitting, compression, and shear) recently. They performed the statistical analysis of the dominant frequencies of AE waveforms and found that the two dominant frequency concentration bands of rocks are located in the ranges of 19 ~ 100 and 181 ~ 270 kHz. By the first motion polarity method and the moment tensor method, these two dominant frequency concentrations were found closely corresponding to the failure modes; that is, the AE waveforms with high dominant frequency (H-type waveforms) are caused by micro-shear failure events, and the waveforms with low dominant frequency (L-type waveforms) are produced by micro-tensile failure events. In this sense, the statistical analysis of the dominant frequencies of AE waveforms is expected to quantify the failure modes of AE sources and further investigate the rock failure progressive process.

Among the environmental parameters affecting rock mechanical behavior and strength, the presence of water is primordial (Erguler and Ulusay 2009; Rabat et al. 2020b). Rock–water interactions have been widely studied because it is meaningful for many applications, e.g., earthquake nucleation, landslide triggering, and reservoir stimulation. Previous studies consistently showed that water-bearing property of rock materials can cause significant decreases in some of their most important mechanical properties such as uniaxial compressive strength (UCS) (Kim et al. 2017; Zhu et al. 2020), uniaxial/Brazilian tensile strength (UTS/BTS) (Cai et al. 2022; Rabat et al. 2023; Zhou et al. 2016), point load strength index (I_s (50)) (Rabat et al. 2020a; Ulusay and Erguler 2012), etc. Further, a plethora of mechanisms has been proposed to explain these strength reductions, including pore water pressure, frictional weakening, and physical and chemical process. However, the respective contribution of these mechanisms to the water weakening of one specific rock is poorly constrained by an effective analytical method. For simple experimental conditions and a defined rock type, it is a rather difficult challenge to evaluate if one (or more) mechanisms prevail over the others. In this condition, the statistical analysis method of the dominant frequencies of AE waveforms was performed in our previous work to interpret the interaction feature of one specific water-weakening mechanism when rock is subjected to compressive loading (Zhu et al. 2020, 2019). We found that the water-weakening mechanisms are closely related to the generation of different types of rock failures. In particular, the pore water pressure causes a dramatic increase in tensile failures due to the enhancement of tensile stress around pores or cracks. The four-point bending loading is believed to drive the fracture of rock in a state of tensile stress (Mardalizad et al. 2017; Wang et al. 2022). Although rock is often subjected to bending loads in practical engineering, study on its micro failure process under water-bearing conditions is limited to date. The spectrum features of rock AE signals under four-point bending conditions are rarely discussed. In this connection, the statistical analysis of the dominant frequency of AE waveform can provide a new perspective on the involving water-weakening reason for the strength degradation of rock under bending loads. More specifically, this approach helps to evaluate the failure modes and interpret the possible contribution of the investigated water-weakening mechanism for rock under four-point bending loading.

The overarching ambition of our work is to shed light on the quantitative analysis of the intrinsic failure characteristic of water-bearing rocks under bending conditions and to further explain the strength degradation in this scenario. Incidentally, the terms "cracking" and "failure" are equivalently used in this paper regardless of their relatively distinct definitions. This paper is organized as follows. First, we present the studied rock materials as well as the experimental and analytical methods adopted for this study. The data processing of AE parameters and waveforms is provided in Sect. 2 in detail. Section 3 presents our main experimental results, and the discussion concerning the findings is given in Sect. 4. Finally, the conclusions are drawn in Sect. 5.

2 Experimental Methodology

2.1 Rock Materials

Two kinds of rock materials including marble and limestone are selected for this study. The marble rock was collected at a marble open-pit mine located in Baoxing County, Sichuan province, China, and the limestone rock was extracted from the reservoir bank slope of Mahu, Leibo County, China. To characterize the tested rocks, X-ray diffraction (XRD) tests were first performed. It revealed that marble and limestone are both entirely composed of calcite minerals. In the experiments, rectangular cuboid samples with dimensions of $150 \times 45 \times 45$ mm^3 (allowable error range of size of ± 0.25 mm) were used. The flatness of each surface of the samples corresponded to a less than 2% error. Table 1 shows the physical and mechanical parameters of these two kinds of rock samples. The natural bulk density ρ and water content w were calculated using traditional techniques by determining weights and sample bulk volume. The longitudinal (P)

Table 1 Summary of physical and mechanical parameters of rock specimens

Rock type	ρ(g/cm^3)	σ(MPa)	E(GPa)	V_p(m/s)	w(%)	Mineral composition
Marble	2.69	54.36	12.09	4367	3.66	Calcite
Limestone	2.63	120.24	21.48	3892	2.24	

ρ the natural bulk density, w water content of saturated rocks, σ the uniaxial compressive strength, E the elastic modulus, V_p P-wave velocity

Table 2 Four-point bending test results of rock samples

Rock type	No	Condition	w(%)	F_f(MPa)	Avg. F_f (MPa)	N_c(%)	Avg. N_c (%)
Marble	MD1	Dry	0	12.41	12.86	82.77	79.19
	MD2		0	13.07		78.46	
	MD3		0	13.68		80.19	
	MD4		0	12.26		75.34	
	MN1	Natural	1.12	12.85	11.50	81.71	80.15
	MN2		1.08	13.64		85.45	
	MN3		1.23	8.19		71.08	
	MN4		1.54	11.32		82.34	
	MS1	Saturated	3.98	8.82	8.49	89.27	87.64
	MS2		3.42	8.26		87.14	
	MS3		3.73	7.84		91.35	
	MS4		3.50	9.05		82.78	
Limestone	LD1	Dry	0	19.35	19.01	85.42	84.25
	LD2		0	20.21		81.06	
	LD3		0	17.42		86.32	
	LD4		0	19.04		84.18	
	LN1	Natural	0.81	16.26	17.73	84.77	84.71
	LN2		0.62	17.33		80.59	
	LN3		1.14	18.80		83.94	
	LN4		0.92	18.52		89.52	
	LS1	Saturated	2.34	13.79	14.21	92.45	91.24
	LS2		2.15	14.23		90.83	
	LS3		2.26	14.76		88.16	
	LS4		2.19	14.07		93.52	

w water content, F_f peak stress (tensile strength), N_c normalized stress at the critical point. Sample no, *ABn* A, rock type, M is marble, and L is limestone, *B* rock condition, D is dry, N is natural, and S is saturated, *n* is the *n*th sample

wave velocity V_p were determined using a signal-emitting-receiving machine at room pressure and temperature. The compressive strength σ and elastic modulus E were measured by uniaxial compression tests of standard cylindrical samples with a size of 100 mm in length and 50 mm in diameter.

In total, 24 rock samples, including 12 marble samples and 12 limestone samples, were produced. The samples of each rock were randomly divided into three groups, corresponding to the dry, natural, and saturated groups and four rock samples were in each group. The specific steps are as follows:

Step 1: Samples in groups 1 and 3 were first placed in an oven at 105 ℃ for 48 h to remove the water inside and cooled down to room temperature. The quality of the samples was then measured. Afterward, samples in group 1 were stored in a sealed container to avoid moisture exchange in the environment before the test.

Step 2: Samples in group 2 were placed in natural moisture air (average temperature: ~ 23 ℃, relative humidity: ~ 76.53%) for over 15 days. Here, we took the average quality of samples in groups 1 and 3 after step 1 as the drying quality and then measured the water content of samples in group 2.

Step 3: Samples in group 3 were soaked in purified water with a pressure of -0.1 MPa for more than 48 h, then static for 4 h. Specifically, we measured the water content of saturated marble and limestone samples (i.e., MS1 and LS1) at

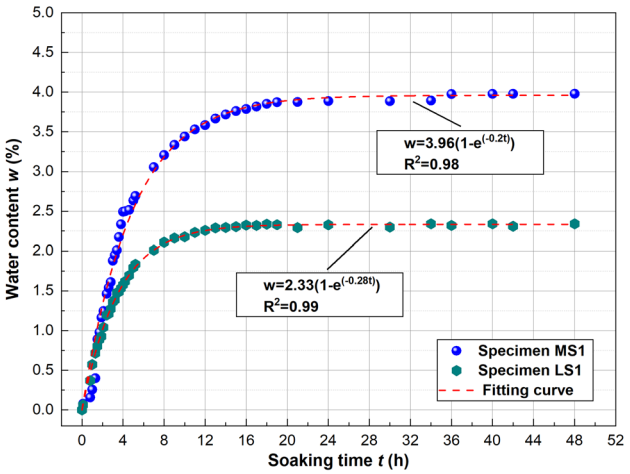

Fig. 1 The water content versus the soaking time of different saturated rock specimens

interval during the soaking process. As shown in Fig. 1, the water content of the marble and limestone samples starts to level off by over 24 and 12 h, respectively. In this sense, samples of group 3 immersed in water for 48 h were believed in a fully saturated state. Note that, the saturated samples in group 3 were kept submerged in water until testing. The water content of all samples is listed in Table 2.

2.2 Four-Point Bending Tests

In the present study, a servo-controlled universal mechanics testing machine (Model: SHT4106) was applied for four-point bending tests, as shown in Fig. 2(a). The capacity of the axial load transducer was 1000 kN. The samples were subjected to symmetric four-point bending by increasing the vertical displacement with a velocity of 0.04 kN/s before the final failure takes place. Note that, samples under blending loads in this study failed without intervention, i.e., no notches were manufactured for the samples.

The AE data were acquired using a PCI-2 eight channels AE collection system (PCA, USA), setting the acquisition threshold to 5 mV and adopting a sampling frequency of 1 Msample/s. Four WDI-AST sensors were deployed to the front and back surfaces of the rock specimen shown in Fig. 2(b). White Vaseline was adopted to enhance the connections between the AE sensors and the sample, with scotch tape to tighten. The WDI-AST sensor used in this study is a resonant-type sensor, which has clear peak sensitivity around its resonant frequency of 125 kHz. The AE waveforms were recorded with triggered mode with an amplitude threshold of 36 dB and were output by the software AEwin for PCI-2. Before the tests, pencil lead break tests were conducted to check the operation condition of the AE monitoring system and AE location accuracy.

2.3 AE Data Processing

2.3.1 AE Characteristic Parameters

The AE characteristic parameters such as counts, energy, and amplitude can be used to evaluate the micro-ruptures and the damage process of rock materials. Specifically, analysis of RA and AF (average frequency), denoted as RA–AF method in this study, is commonly implemented to determine the rock cracking mode. The RA and AF values of AE signals are described (Aggelis et al. 2011):

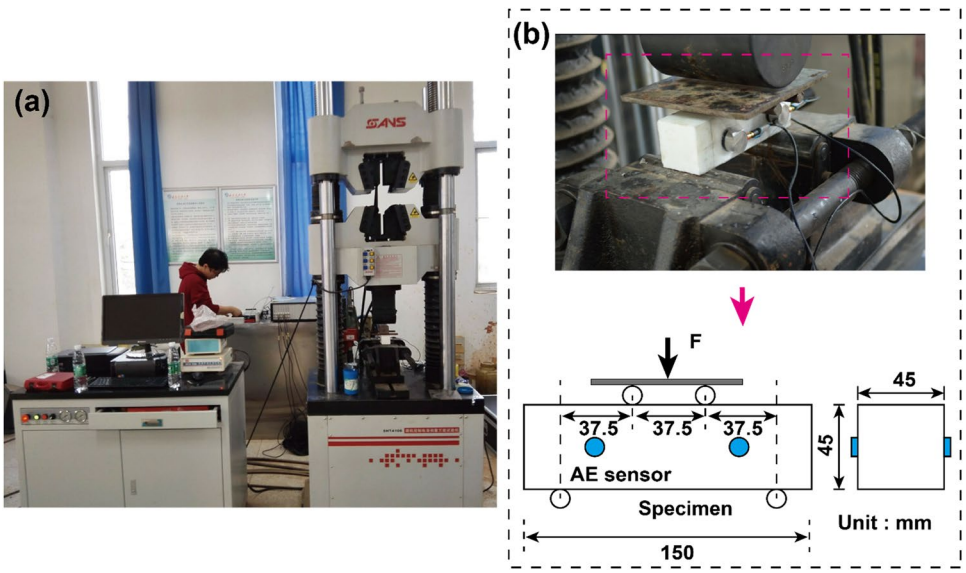

Fig. 2 The four-point bending loading setup, **a** photographic view of loading system, **b** sample size and layout of AE sensors

$$RA = \frac{T_r}{A_m} \tag{1}$$

$$AF = \frac{N}{T_d} \tag{2}$$

where T_r and T_d are the rise time and duration time of the AE signal, respectively, N is the AE counts, and A_m is the maximum amplitude.

According to the relationship between the RA and AF values established, the cracking events could be classified into tensile cracking and shear cracking. A low RA value associated with a high AF value results from the occurrence of tensile cracking, while a higher RA value associated with a lower AF value is caused by the generation of shear cracking.

Figure 3(a) shows the typical evolution of AE counts and cumulative AE counts of rocks (i.e., dry marble sample MD1) during the entire loading process. Due to the abrupt fracture of rock samples under four-point bending conditions, the release of AE counts tends to be concentrated when approaching peak stress. Given this, we defined the moment when dramatic growth of the amount of AE counts (onset of the upward trend of the cumulative AE count curve) occurs as the critical point C' in this study. The generation of AE events before C' is more likely attributed to the friction between rock samples and equipment at the initial loading phase or the closure of primary defects in rock samples. In this line, we focused on the AE counts recorded after C' and further conducted the cracking mode classification in the following study. Figure 3(b) depicts the typical scatter diagrams between the RA value and AF of MD1. One can observe that the RA–AF values were mostly distributed along the longitudinal axis, indicating the dominant role of tensile cracking. Further, the transition line is used to determine the actual number of tensile cracking and shear cracking. Note that the slope of the transition line k is found to vary with the types and conditions of materials. In most previous literature (Ohno and Ohtsu 2010), k was evaluated by the empirical relationship of researchers. An optimal method of determining k for different rocks under various conditions is demanding.

2.3.2 Frequency of AE Waveforms

AE waveform data were recorded in real time during the whole test. Given the close relationship between the frequency characteristic of the AE waveform signals and the cracking mechanism, spectrum analysis was conducted in this study. As shown in Fig. 4(a), the conversion of the AE waveform from the time domain to the frequency domain could be conducted via the fast Fourier transform (FFT). With the help of MATLAB software, the frequency corresponding to the maximum amplitude, the dominant frequency in Fig. 4(a) namely, was determined, with a value of 15 kHz. Noteworthy, a batch program was developed to process numerous waveform data and obtain their dominant frequency efficiently in this study.

Since the dominant frequencies of AE signals released by rock fracturing are mostly distributed in the range of 0 ~ 500 kHz, a criterion for dividing the dominant frequency for each sample was proposed. That is, the dominant frequencies lower than 450 kHz were grouped into 45 bands with a constant interval of 10 kHz, and others were divided into the 46th band. Further, we counted the number of dominant frequencies in each band and calculated their percentage. For all the tested rock samples, there is an apparent feature of two concentrations in dominant frequency bands, regardless of the water contents. As shown in Fig. 4(b), these two concentrations of dominant frequency bands were named high dominant frequency bands (H-type bands) and low dominant frequency bands (L-type bands). Correspondingly, the AE waveforms located in H-type and L-type bands were named H-type waveforms and L-type waveforms. In this sense, we selected the dominant frequency bands whose percentage is more than 1% and calculated the percentages of H-type and L-type waveforms, which could be conducive to the following analysis.

3 Experimental Findings

3.1 Variation of Mechanical Properties Due to Water Bearing

The peak stress F_f (MPa), denoted as tensile strength, was calculated through Eq. (3).

$$F_f = \frac{FL}{bh^2} \tag{3}$$

where F is the maximum force, L is the length of the specimen, b and h are the length and height of the cross-sectional area.

For all tested marble and limestone under different water contents, the mechanical results of the four-point bending experiments follow an abrupt deformation when they approach the peak stress (for instance, the case shown in Fig. 3(a)). In this study, we evaluated the correlation between water content and two kinds of stress, including peak stress and stress at the critical point C'. As shown in Fig. 5(a) and Table 2, the peak stress of rock samples decays with increasing water content. Both two rocks present lower peak stress under water-saturated conditions as

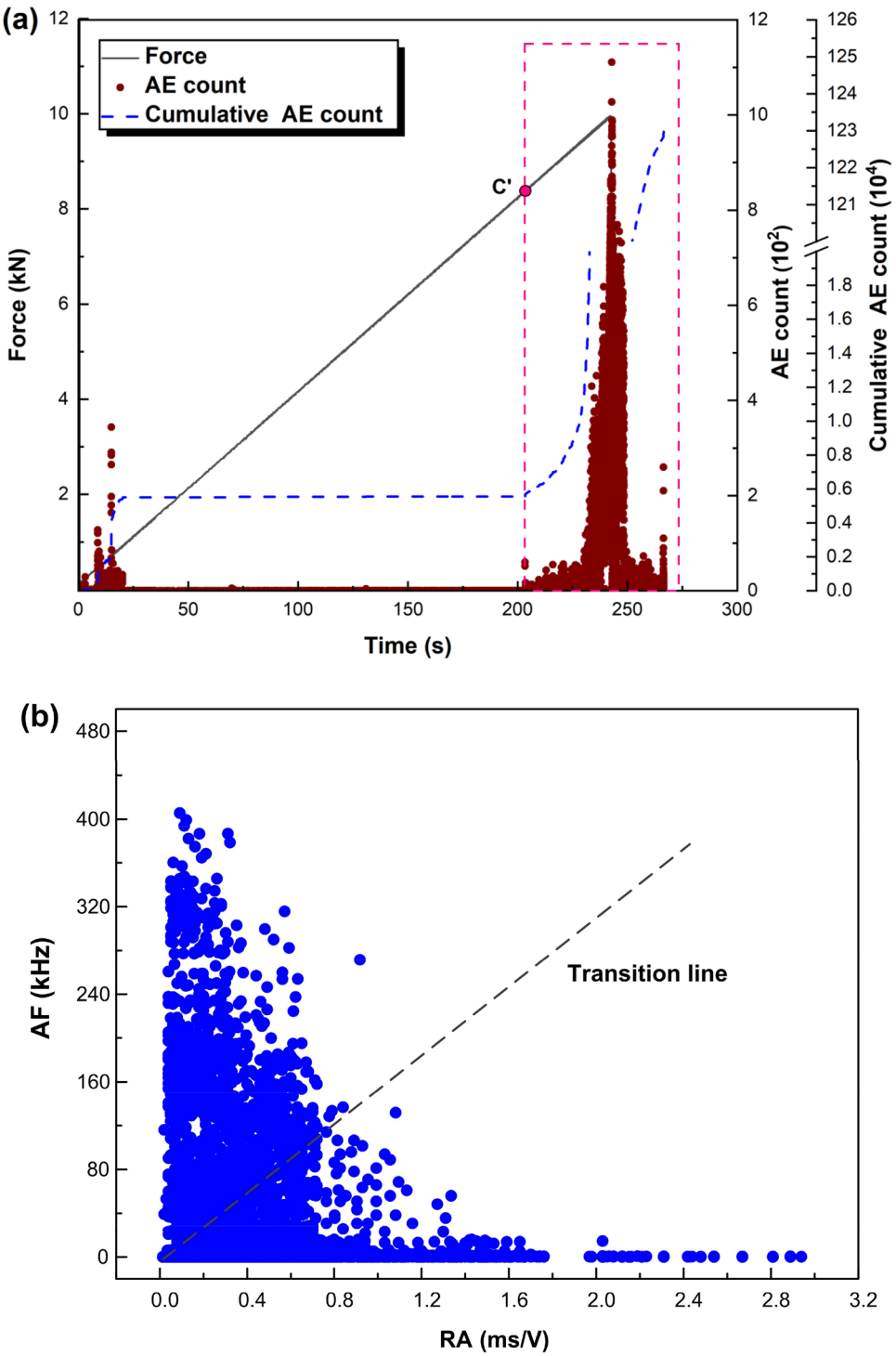

Fig. 3 The AE counts accumulation and its RA–AF distribution, **a** AE counts accumulation, and **b** distribution of RA–AF for AE counts generated during rock fracture

opposed to dry conditions, i.e., water weakening. Under water-saturated conditions, the tensile strength of marble and limestone samples is 66.06 and 74.78% of that observed in the dry experiments on average, respectively. This suggests that both marble and limestone are characterized by strong water weakening, with the former being more obvious. Moreover, fewer reductions in tensile strength for natural rocks, i.e., 10.54 and 6.72% for marble and limestone, respectively, can be found when compared to saturated rocks. This may be attributed to its relatively lower water content, resulting in less mechanical degradation.

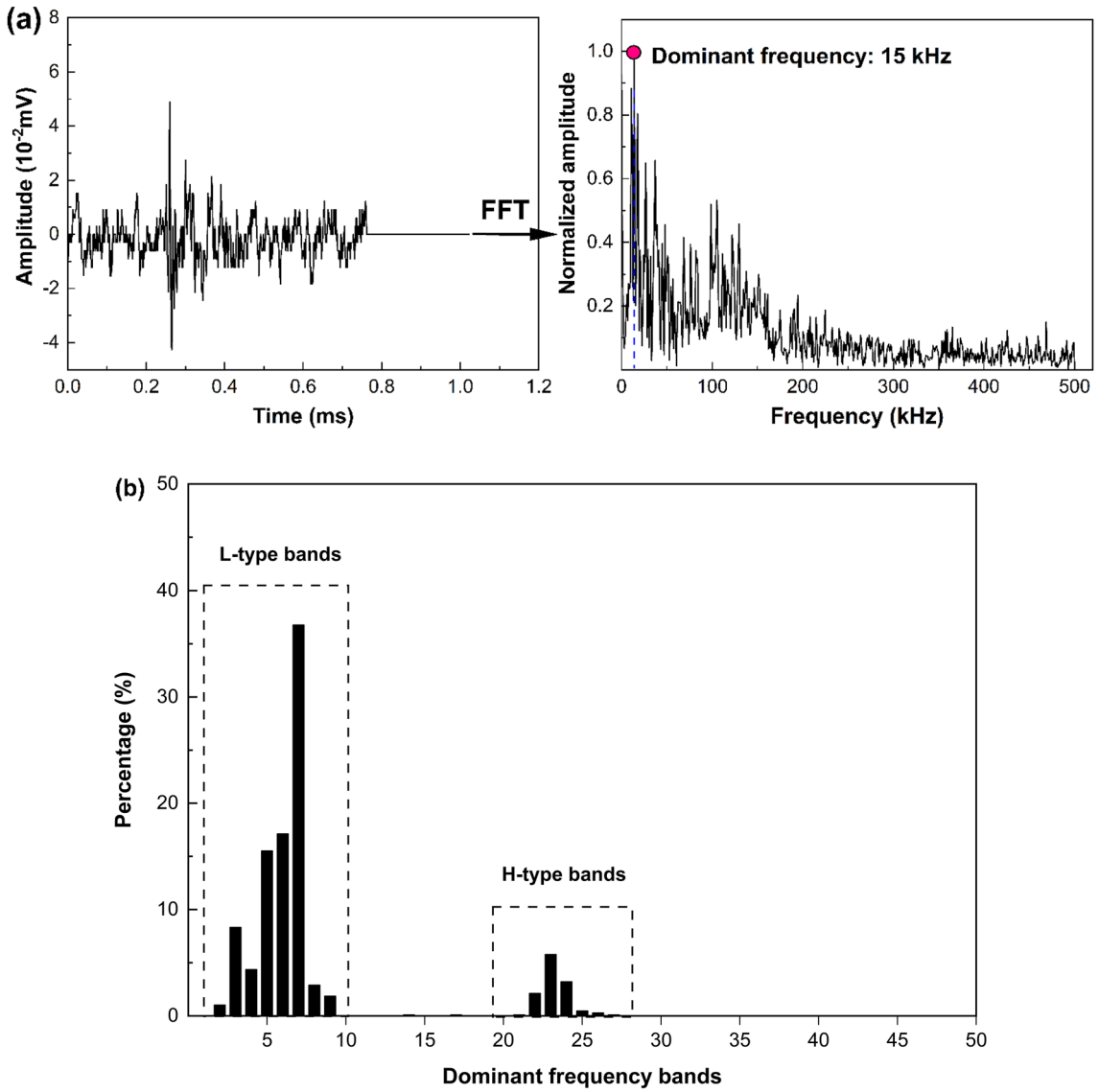

Fig. 4 Data processing of AE waveforms, **a** extraction process of the dominant frequency of AE waveforms, and **b** percentages of AE waveforms distributed in different dominant frequency bands

The normalized stress at the critical point N_c is defined as the ratio between the stress at C' and the peak stress in this study. In general, N_c is an increasing function of the water content (Fig. 5(b)). The water-saturated rock samples experience obvious cracking propagation at a higher value of N_c than dry rock samples. Indeed, N_c under water-saturated conditions is 8.45 and 6.99% higher than under dry conditions for marble and limestone, respectively. The N_c is, however, very close under dry and natural conditions, showing increments of 0.96 and 0.46% for marble and limestone, respectively. The increments in N_c of two rocks under different conditions indicate that the presence of water delays the occurrence of numerous cracking, and the higher the water content, the more delayed the obvious cracking activities. The phenomenon can be attributed to the water-weakening effect, e.g., friction weakening, which makes some crackings fail to monitor by lowering their energy.

The percentages of H-type and L-type waveforms of rock samples were plotted against the water contents, as shown in Fig. 5(c). The results suggest that the L-type waveform hosts the AE waveform signals released, and its dominant role did not affect by rock types and water conditions. A mutually inhibiting relationship between the percentages of H-type waveforms and L-type waveforms could be observed, manifesting that the sum of them is almost equal to 100%. Overall, the percentages of L-type waveforms were found to increase when water content

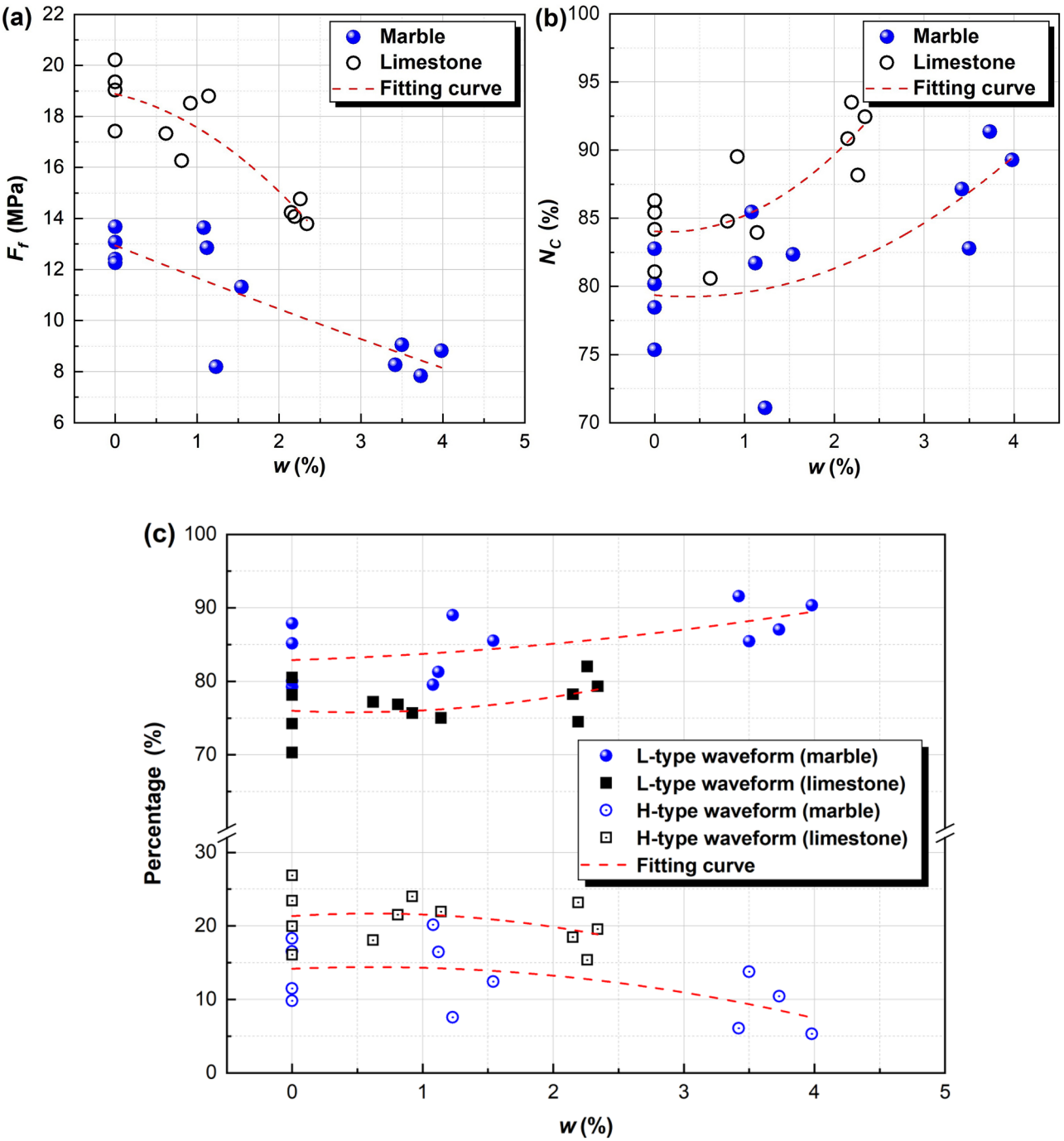

Fig. 5 The variations of stress and percentages of AE waveforms with water contents of rocks under the four-point bending condition, **a** peak stress, **b** normalized stress at C', and **c** percentages of H-type and L-type waveforms

increased, and the percentages of H-type waveforms, as would be expected, showed decreasing trends. The percentages of L-type waveforms are 5.51 and 2.71% greater for marble and limestone samples on average under water-saturated conditions compared to dry conditions, and those are 0.74 and 0.38% greater under natural conditions compared to dry conditions, respectively. In addition, the percentages of L-type waveforms in marble rock are generally greater than that in limestone rock, and the percentages of H-type waveforms exhibit an opposite trend.

3.2 Cracking Behavior Analysis Based on Acoustic Emission

To further investigate the cracking features from the AE perspective, we connected the dominant frequencies of AE waveforms and failure events determined by RA–AF distribution. As mentioned in Sect. 2.3.1, percentages of tensile and shear failures can be determined when the slope of transition line k is set. In this study, we set the k value as 100, 150, and 200 since the k is approximately from 1 to 500 for rocks under different loading conditions based on the previous study (Zhu et al. 2022). As shown in Fig. 6, the results demonstrated that the increasing k for two rocks under different water contents produced a remarkable decrease in the average percentage of tensile failures, but caused an increase in the average percentage of shear failures. Interestingly, the percentages of AE waveforms distributed in different dominant frequency bands and the failure modes are close; that is, the H-type waveforms typically correspond to shear failures and L-type waveforms match the tensile failures well. This finding emphasized a corresponding relationship between the dominant frequency feature and failure modes.

Another finding is that, unlike the dominant frequency types of AE waveforms, no apparent dependence of the percentages of failure on water contents could be found when a constant k was set. Taking the L-type waveforms and tensile failures as examples, the percentages of L-type waveforms increase with increasing water contents, while the positive correlation between tensile failure and water content is not observed in some scenarios, e.g., $k = 150$ and $k = 200$ for marble rock. This suggests that water content affects the optimal selection of k value if the results of dominant frequencies of AE waveforms are taken as baseline. The corresponding relationship between the dominant frequency feature and failure modes for rocks under dry and natural conditions is most pronounced when the k is set as 200, and this for saturated rocks happens when the k is set as 150. This is in agreement with our previous study on marble under direct tension, where the optimal k is 150 for dry and natural marble and 100 for saturated marble (Zhu et al. 2022). In this sense, we can conclude that the rock condition and loading regime both have significant effects on the optimal selection of k value.

3.3 Dependence of Failure Component on Rock Strength

The micro-tensile failure is expected to character the rock strength since it dominates the rock fracture under four-point bending. Figure 7 depicts the correlation of rock strength with the percentage of tensile failure P_t of two rocks. Rock tensile strength is found to be a decreasing function of the percentage of tensile failure, and their relationship was modeled using the quadratic polynomial function. It means that a less percentage of micro-tensile failure can cause a greater tensile strength. Note that the negative correlation of F_f with P_t holds for marble or limestone or a combination of both. This finding is consistent with the well-known behavior in which the ability of a brittle rock to compress is much greater than that to stretch. This being said, the less tensile failure generation may be a reasonable explanation for rock tensile strength enhancement.

In the present study, we statistically propose the factors m and n to evaluate the contributions of micro-cracks produced by tensile and shear failures to the tensile strength, which is shown in Eq. (4):

$$F_f = mP_t + nP_s \tag{4}$$

where P_t and P_s indicate the percentage of tensile failure events and shear failure events, respectively.

To determine the m and n, original data derived from dry and saturated groups are regarded as known quantities. For marble rock, the average percentages of tensile failure of dry and saturated samples are 83.09 and 88.61%, and their average tensile strength is 12.86 and 8.49 MPa, respectively. Hence, Eq. (5) can be described as follows:

$$\begin{cases} 0.8309m + 0.1691n = 12.86 \\ 0.8861m + 0.1139n = 8.49 \end{cases} \tag{5}$$

Therefore, the factors for marble rock can be obtained as: $m = -0.53$, $n = 78.61$.

Similarly, we determined the factors for limestone rock by utilizing the parameters under dry and saturated conditions (percentages of micro-tensile failure events: 75.82 and 78.53%, tensile strength: 19.01 and 14.21 MPa). The factors for limestone rock are determined as $m = -23.76$, $n = 153.08$.

Then the original data for the dry and saturated rock samples are used to predict the tensile strength of natural rock samples and to verify the accuracy of these two factors. Using the factors m and n, a prediction of strength for natural rocks can be conducted on the percentage and its average value of micro failure as Eq. (4). The predicted strength of natural marble and limestone and their prediction error are shown in Fig. 8. It is evident that the prediction errors of all samples are less than 15%, indicating a high prediction accuracy. To be specific, the absolute values of prediction errors for natural marble vary from 0.03 to 14.86%, and those for natural limestone vary from 3.91 to 8.47%, respectively. Moreover, the average failure component can be used to predict their average strength on the premise of knowing factors m and n. The predicted strength is 12.27 MPa for natural marble and 18.33 MPa for natural limestone. Compared to the average measurement, the errors of the predicted

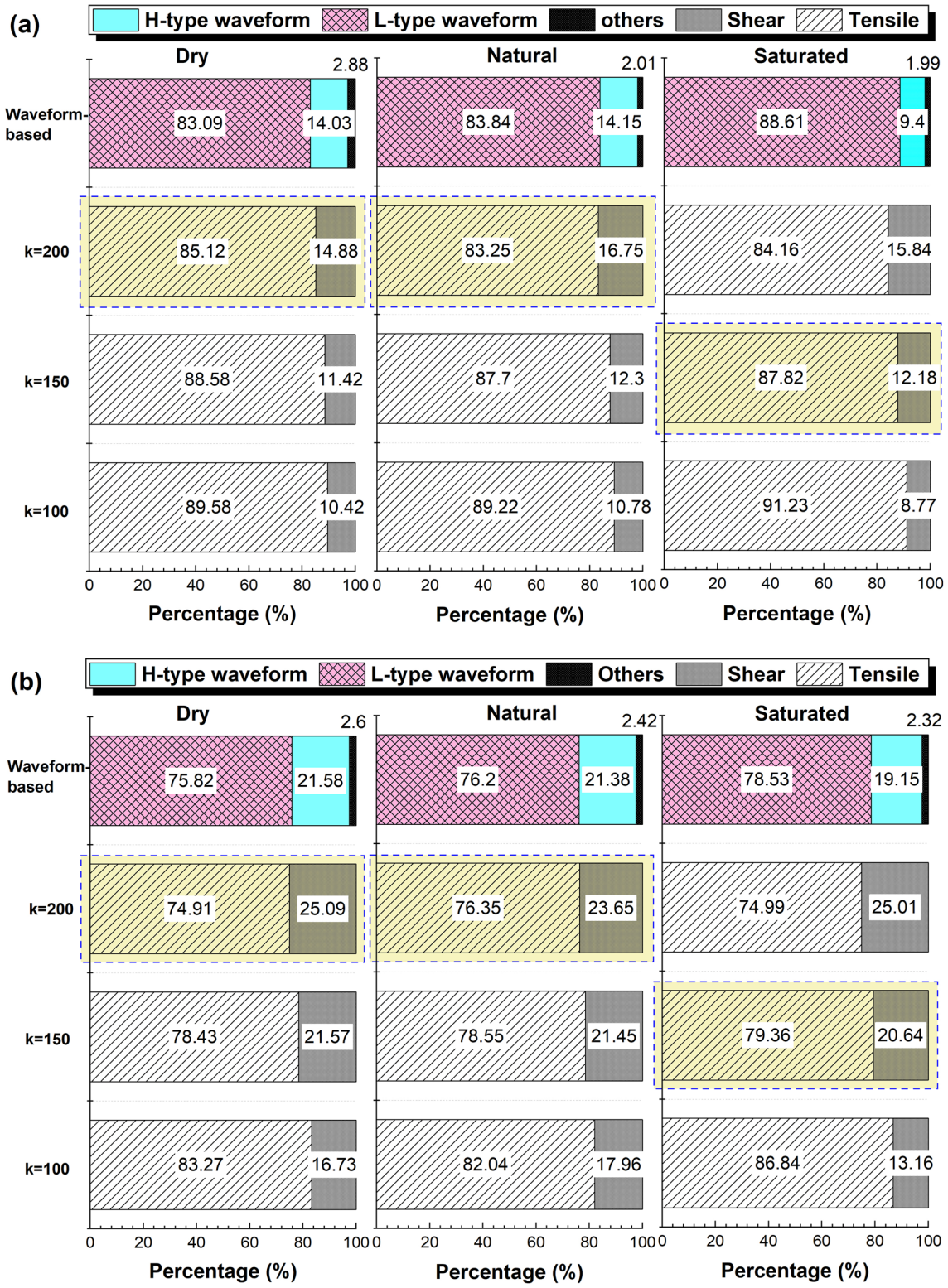

Fig. 6 The correlation of failure modes and AE waveform types, **a** marble, and **b** limestone. The boxes with light yellow backgrounds represent the optimal *k* value of rocks under different conditions

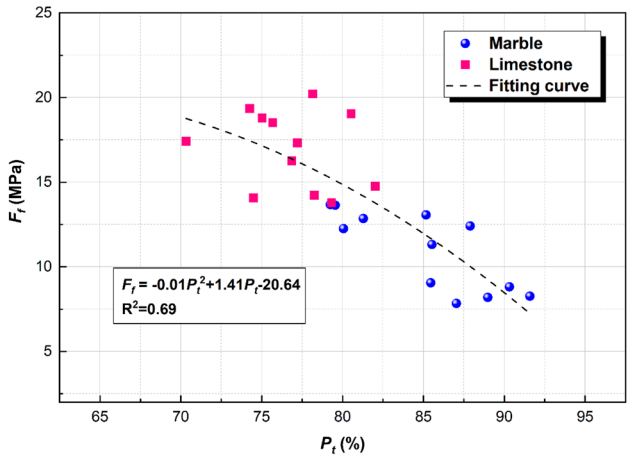

Fig. 7 The variation of tensile strength with the percentage of tensile failure of different rocks

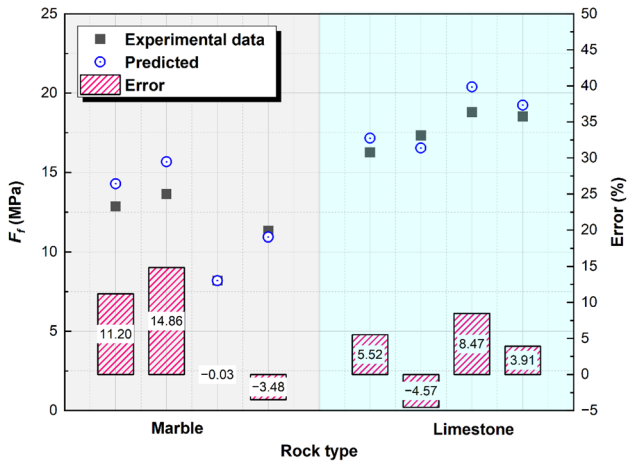

Fig. 8 Comparison between experimental and predicted strength of different natural rocks. The prediction errors are calculated following the experimental values as the baseline. Compared to the experimental strength, a positive prediction error indicates a greater predicted strength, and a negative prediction error means a lower predicted strength

value of marble and limestone are calculated as 6.67 and − 3.42%, respectively. All these observations highlighted that the factors *m* and *n* established are accurate and effective for predicting the tensile strength of two tested natural rocks.

4 Discussion

AE sensing is expected to identify the rock failure modes since the generated wave is closely relevant to physical processes such as the source mechanism. Compared to the AE parameters in the time domain, the spectral characteristics, i.e., the dominant frequency of the AE waveform, are often thought to be more reflective of the essential rock fracturing. In this case, it is reasonable to speculate that the dominant frequency of the AE waveform may be able to interpret some vital features of rock fracturing, e.g., the failure modes. Extensive previous studies have found two dominant frequency bands of AE waveforms released when rocks are subjected to compression, shear, and direct tension (Deng et al. 2018; Huang et al. 2019; Li et al. 2017; Li 2017; Wang et al. 2019; Zhu et al. 2020). The similar result obtained in this study enriches the applicable loading and rock conditions (i.e., four-point bending and water bearing, respectively) of two dominant frequency bands of AE waveforms.

The foremost outcome derived from this work was the obvious quantitative correspondence between the types of AE waveforms and the failure modes determined by the RA–AF method. Given the results of dominant frequencies of AE waveforms, the slope of the transition line *k* in the RA–AF method can be determined, along with the exact number of the two kinds of failures further. Since different *k* was adopted to classify the rock failure modes by empirical relationship in previous literature (Aggelis 2011; Wang et al. 2017), the quantitative analysis based on dominant frequencies of AE waveforms in this study could remove subjective judgment and contribute to the reliability of the AE source mechanism. Additionally, the optimal *k* varies with the rock conditions, i.e., 200 for dry and natural rocks, and 150 for saturated rock. This means the presence of water affects the generation of different types of rock failures. In this sense, the effect of water, which attributes to rock strength reduction, can be equivalent to the failure component associated with it. Hence, predicting the rock strength by resolving equations constituted by components of tensile and shear failures in Sect. 3.3 is believed to be reasonable and reliable. A practical situation is that both dry and saturated procedures of rock are easy to implement in the laboratory, while the natural condition closely related to practical engineering is difficult to maintain, due to the effects of changing ambient temperature and humidity. On the premise of high accuracy, the predicting tensile strength of natural rock by fitting data of dry and saturated rocks in this study can be used as a design parameter for rock engineering, e.g., rock slab structure in construction.

The fact that water bearing can cause rock mechanical deterioration, e.g., strength loss, has been accepted for decades. However, the mechanisms used to explain such water weakening, which depends on a defined set of conditions (i.e., temperature and strain rate) and/or rock type, are diverse and complex. In particular, the following causes are proposed in previous studies: pore water pressure increase, friction weakening, fracture energy decrease, and chemical and corrosive deterioration (Baud et al. 2000; Erguler and Ulusay 2009). Out of these possible causes, friction weakening and the fracture energy reduction could be extrapolated

as the two main reasons for strength degradation in the two rocks studied as the pore water pressure increase, and chemical and corrosive deterioration would be very limited in this scenario because of rock composition and loading regime.

The friction coefficient, which is characterized by the shear stress normalized by the normal stress acting on a rock surface at the onset of sliding, is often utilized to assess rock friction; it is generally found to reduce in the presence of water (Dieterich and Conrad 1984; Zhang et al. 2019). Two possibilities are mainly responsible for this reduction: (1) water diminishes the adhesion forces at contact points, and (2) water decreases the strength of the asperities supporting the shear stress. The fracture energy reduction, which is based on Griffith's fracture criterion, holds that water reduces the energy required per unit for the advance of cracks, and tensile stress further promotes crack growth (Rehbinder and Shchukin 1972). It has been documented by previous studies to originate from mineral dissolution, capillary forces at the crack tip, clay weakening, grain contact lubrication, stress corrosion, or a reduction of surface energy. Among them, stress corrosion is the replacement of silica-oxygen bonds by weaker hydrogen bonds within the quartz or silicate lattice, and causes a reduction of the stress threshold of crack growth (Atkinson and Meredith 1981; Nara et al. 2011). In this connection, it should be recalled that the tested marble and limestone are both composed of pure calcite. The clay weakening and stress corrosion would be of little significance as the two rocks studied both absent from clay and silicious minerals. Moreover, due to the low process of solubility of calcite in water (Rabat et al. 2021; Risnes et al. 2005), these two tested rocks exposed to water for very short periods of test time were believed to experience weak dissolution. Hence, the capillary forces at the crack tip, grain contact lubrication, or surface energy reduction could be responsible for one part of the observed weakening. The numerous L-type waveforms recorded are reliable indicators for massive tensile failures, supporting the prevailing tensile stress state inside rock. According to Griffith's fracture criterion, the existing tensile stress state makes the exertion of fracture energy reduction plausible. However, the mechanisms involved in the water weakening of the frictional weakening and fracture energy reduction are complex, and future experimental investigations are needed to better constrain the processes.

5 Conclusion

In this study, the failure mode classification of water-bearing marble and limestone under four-point bending conditions was performed based on a quantitative AE method, that is, the combination of AE parameters and the dominant frequencies of AE waveforms. Given the water-bearing effects on the generation of failure components, the tensile strength of natural rocks was predicted by fitting data (i.e., tensile strength, percentages of tensile and shear failures) of dry and saturated rocks, and the reliability of this prediction was verified. The most important results derived from this work are as follows:

(1) Substantial reductions in tensile strength were obtained when moisture increased in the two rocks, especially for marble rock. The presence of water causes the occurrence of obvious microcracking delay.
(2) The dominant frequencies of AE waveforms were characterized by the distribution of two concentrations. There is an apparent correspondence between the two dominant frequency bands and failure modes classified by the RA–AF method. Further, the two dominant frequency bands of AE waveforms could be used as a baseline for the failure mode classifications in the RA–AF method by determining the optimal slope of the transition line.
(3) The water-bearing effect on rock tensile strength can be equivalent to the failure components associated with it. The predicting tensile strength of natural rocks by equations originating from the data of dry and saturated rocks is proved to be accurate with general slight errors.
(4) The mechanisms of water weakening on rock tensile strength in four-point bending tests can be linked to friction weakening and fracture energy reduction. The clay weakening, mineral dissolution, and stress corrosion are of little significance due to the rock composition and loading regime.

Acknowledgements This work was supported by the National Natural Sciences Foundation of China (Grant Nos. U19A2098, U19A2049, 41772322) and the Natural Sciences Foundation of Sichuan Province (Grant No. 2023NSFSC0786). The authors are very grateful for the financial contribution and convey their appreciation for supporting this basic research.

Declarations

Conflict of Interest The authors declare that there is no conflict of interest regarding the publication of this article.

References

Aggelis DG (2011) Classification of cracking mode in concrete by acoustic emission parameters. Mech Res Commun 38(3):153–157
Aggelis D, Kordatos E, Matikas T (2011) Acoustic emission for fatigue damage characterization in metal plates. Mech Res Commun 38(2):106–110

Atkinson BK, Meredith PG (1981) Stress corrosion cracking of quartz: a note on the influence of chemical environment. Tectonophysics 77(1–2):T1–T11

Baud P, Zhu W, Wong TF (2000) Failure mode and weakening effect of water on sandstone. J Geophys Res: Solid Earth 105(B7):16371–16389

Cai X, Cheng C, Zhao Y, Zhou Z, Wang S (2022) The role of water content in rate dependence of tensile strength of a fine-grained sandstone. Arch Civ Mech Eng 22(1):1–16

Chugh YP, Hardy HR, Stefanko R (1968) Investigation of the frequency spectra of microseismic activity in rock under tension. The 10th US Symposium on Rock Mechanics (USRMS) at the universtiy of Texas at Austin. Applied Rock Mechanics 20–22:73–113

Deng J, Li L, Chen F, Yu J, Liu J (2018) Twin-peak Frequencies of Acoustic Emission Due to the Fracture of Marble and Their Possible Mechanism. Adv Eng Sci 50(5):12–17

Dieterich JH, Conrad G (1984) Effect of humidity on time-and velocity-dependent friction in rocks. J Geophys Res: Solid Earth 89(B6):4196–4202

Erguler ZA, Ulusay R (2009) Water-induced variations in mechanical properties of clay-bearing rocks. Int J Rock Mech Min Sci 46(2):355–370

He M, Zhao F, Zhang Y, Du S, Guan L (2015) Feature evolution of dominant frequency components in acoustic emissions of instantaneous strain-type granitic rockburst simulation tests. Rock and Soil Mechanics 36(1):1-8,33

Huang Y, Deng J, Zhu J (2019) An experimental investigation of moisture-induced softening mechanism of marble based on quantitative analysis of acoustic emission waveforms. Appl Sciences-Basel 9(3):AN:446

Jia X (2013) Experimental study on acoustic emission Eigen-frequency spectrum features of strain bursts. China University of Mining and Technology, Beijing

Kim E, Stine MA, de Oliveira DBM, Changani H (2017) Correlations between the physical and mechanical properties of sandstones with changes of water content and loading rates. Int J Rock Mech Min Sci 100:255–262

Li LR (2017) Dominant frequencies and their mechanical mechanism of acoustic emissions in rock failures. Sichuan University, Chengdu

Li C, Nordlund E (1993) Assessment of damage in rock using the Kaiser effect of acoustic emission. Int J Rock Mech Min Sci Geomech Abstracts 30(7):943–946

Li L, Deng J, Zheng L, Liu J (2017) Dominant frequency characteristics of acoustic emissions in white marble during direct tensile tests. Rock Mech Rock Eng 50(5):1337–1346

Manthei G, Eisenblätter J (2008) Acoustic emission in study of rock stability. Acoustic emission testing, Springer, Berlin, Heidelberg, p.: 239–310.

Mardalizad A, Scazzosi R, Manes A, Giglio M (2017) Four-point bending test on a middle strength rock: numerical and experimental investigations. Frattura Ed Integrità Strutturale 11(41):504–523

Nara Y, Morimoto K, Yoneda T, Hiroyoshi N, Kaneko K (2011) Effects of humidity and temperature on subcritical crack growth in sandstone. Int J Solids Struct 48(7–8):1130–1140

Ohno K, Ohtsu M (2010) Crack classification in concrete based on acoustic emission. Constr Build Mater 24(12):2339–2346

Rabat Á, Cano M, Tomás R, Tamayo ÁE, Alejano LR (2020a) Evaluation of strength and deformability of soft sedimentary rocks in dry and saturated conditions through needle penetration and point load tests: a comparative study. Rock Mech Rock Eng 53(6):2707–2726

Rabat Á, Tomás R, Cano M (2020b) Evaluation of mechanical weakening of calcarenite building stones due to environmental relative humidity using the vapour equilibrium technique. Eng Geol 278:105849

Rabat Á, Tomás R, Cano M (2021) Advances in the understanding of the role of degree of saturation and water distribution in mechanical behaviour of calcarenites using magnetic resonance imaging technique. Constr Build Mater 303:124420

Rabat Á, Tomás R, Cano M (2023) Assessing water-induced changes in tensile behaviour of porous limestones by means of uniaxial direct pull test and indirect methods. Eng Geol 313:106962

Rehbinder PA, Shchukin ED (1972) Surface phenomena in solids during deformation and fracture processes. Prog Surf Sci 3:97–188

Risnes R, Madland M, Hole M, Kwabiah N (2005) Water weakening of chalk—Mechanical effects of water–glycol mixtures. J Petrol Sci Eng 48(1–2):21–36

Rodríguez P, Celestino TB (2019) Application of acoustic emission monitoring and signal analysis to the qualitative and quantitative characterization of the fracturing process in rocks. Eng Fract Mech 210:54–69

Ulusay R, Erguler Z (2012) Needle penetration test: evaluation of its performance and possible uses in predicting strength of weak and soft rocks. Eng Geol 149:47–56

Wang H, Xian X, Yin G, Xu J (2000) A new method of determining geostresses by the acoustic emission Kaiser effect. Int J Rock Mech Min Sci 37(3):543–547

Wang M, Tan C, Meng J, Yang B, Li Y (2017) Crack classification and evolution in anisotropic shale during cyclic loading tests by acoustic emission. J Geophys Eng 14(4):930–938

Wang Y, Deng J, Li L, Zhang Z (2019) Micro-failure analysis of direct and flat loading brazilian tensile tests. Rock Mech Rock Eng 52(11):4175–4187

Wang Z, Qin W, Gao Y, Yang Y, Lv H, Zhang L (2022) Investigations on fatigue properties of red sandstone under positive and negative pure bending loads. Constr Build Mater 321:126379

Zhang N, Qi Q, Ouyang Z, Li H, Zhao S, Xiu Z (2014) Experimental on acoustic emission characteristics of marble with different stress paths. J China Coal Soc 39(2):389–394

Zhang B, Liu W, Deng J, Liu J (2016) Damage mechanism and stress wave spectral characteristics of rock under tension. Chinese J Geotech Eng 32(2):336–341

Zhang Q, Li X, Bai B, Hu H (2019) The shear behavior of sandstone joints under different fluid and temperature conditions. Eng Geol 257:105143

Zhou Z, Cai X, Cao W, Li X, Xiong C (2016) Influence of water content on mechanical properties of rock in both saturation and drying processes. Rock Mech Rock Eng 49(8):3009–3025

Zhu J, Deng J, Huang Y, Yu Z (2019) Experimental study on characteristic strength of saturated marble. Chin J Rock Mech Eng 38(6):1129–1138

Zhu J, Deng J, Chen F, Huang Y, Yu Z (2020) Water saturation effects on mechanical and fracture behavior of marble. Int J Geomech. https://doi.org/10.1061/(ASCE)GM.1943-5622.0001825

Zhu J, Deng J, Chen F, Wang F (2022) Failure analysis of water-bearing rock under direct tension using acoustic emission. Eng Geol 299:106541